

Obtaining two attosecond pulses for x-ray stimulated Raman spectroscopy

A. Zholents and G. Penn

Lawrence Berkeley National Laboratory, Berkeley, California, 94720, USA

ABSTRACT

Attosecond x-ray pulses are an indispensable tool for the study of electronic and structural changes in molecules undergoing chemical reactions. They have a wide bandwidth comparable to the energy bands of valence electronic states and, therefore, are well suited for making and probing multiple valence electronic excitations using core electron transitions. Here we propose a method of creating a sequence of two attosecond soft x-ray pulses in a free electron laser by optical manipulation of electrons located in two different sections of the electron bunch. The energy of each x-ray pulse can be of the order of 100 nJ and the pulse width of the order of 250 attoseconds. The carrier frequency of each x-ray pulse can be independently tuned to a resonant core electron transition of a specific atom of the molecule. The time interval between the two attosecond pulses is tunable from a few femtoseconds to a hundred femtoseconds with better than 100 attoseconds precision.

PACS numbers 41.60.Cr, 42.55.Vc

1. Introduction

Chemical bonds form, break or change on a time scale of femtoseconds [1]. The advent of extreme ultraviolet attosecond pulses produced with the technique of high harmonic generation in a gas (see [2] and references therein) have opened up the possibility for direct study of these processes. Promising ideas for the generation of intense soft x-ray and hard x-ray attosecond pulses using free electron lasers (FELs) [3-11] were also proposed. More recently another scheme for the generation of attosecond x-ray pulses with some similarity to the technique discussed in this paper was presented [12]. Building upon this development, we propose a method to achieve the requirements of a newly proposed technique [13] for the study of the evolution of valence electronic wave packets responsible for the making or breaking of the chemical bonds using stimulated x-ray Raman spectroscopy. It exploits an inherent feature of Fourier-transform limited attosecond x-ray pulses, namely a wide bandwidth comparable to the energy width of valence electronic states in molecules. In the proposed experiment, the first attosecond x-ray pulse with the carrier frequency tuned to a ground state transition of one atom of the molecule creates an electronic wave packet of valence electrons that is later probed by the second attosecond x-ray pulse with the carrier frequency tuned to a ground state transition of the other atom of the molecule. The atom specificity helps to define where the wave packet of valence electrons is created and where it is probed, which simplifies the analysis of the experiment and aids in understanding the spatial distribution of the valence electron wave packets. Evidently, individual measurements done with each pair of the x-ray pump and the x-ray probe pulses and with various and well controlled time

delays between the pulses combine into a motion picture showing the dynamics of changes in chemical bonds.

To the best of our knowledge, the production of only one attosecond x-ray pulse has been addressed in the literature so far, but two pulses are needed for the above described experiment. In principle, one attosecond x-ray pulse can be split into two pulses and an adjustable time delay can be provided, but these pulses will have the same carrier frequency as the parent pulse and, thus, can only be used for pumping and probing on the same atom.

Here we propose a method of production of a sequence of two attosecond x-ray pulses with two different carrier frequencies. Also implemented is a possibility to adjust the time delay between the first and the second pulse with a high precision. In the first part of the paper we describe the basic idea of the method and illustrate it in the second part with a numerical example. In this example, we demonstrate the feasibility of generation of two x-ray pulses with ~ 250 attosecond FWHM tuned to the K-edges of oxygen and nitrogen atoms often jointly appearing in molecules.

2. Method

In the scheme shown in Figure 1 we combine two recent ideas, i.e. proposals of the current enhanced self amplified spontaneous emission [14] and echo enabled microbunching [15]. We begin from the electron beam interaction with the laser field with a carrier frequency ω_1 in a wiggler magnet W1 containing approximately 10 periods. The magnet has period λ_{w1} and undulator parameter $K_{w1} = eB\lambda_{w1}/(2\pi mc)$,

where B is the peak magnetic field, e, m is the electron charge and mass, c is the speed of light, and the undulator parameter has been chosen to match the FEL resonance at the wave length $\lambda_1 = \lambda_{w1} (1 + K_{w1}^2 / 2) / 2\gamma^2$; the corresponding wave vector $q_1 = \omega_1 / c$, where $\gamma = E / mc^2$ and E is the electron beam energy. This interaction produces a modest energy modulation of electrons with a normalized amplitude $a_1 = \Delta E_1 / \sigma_E$, where ΔE_1 is the peak electron energy gain in the wiggler due to interaction with the laser and σ_E is the rms energy spread in the electron bunch. It is assumed here, and in two other cases where interaction of the electrons with the laser light is used, that the crossover of the laser light in the wiggler is several times larger than the horizontal and vertical rms sizes of the electron bunch and thus all electrons at the same location along the electron bunch receive equal energy change according to the phase of the laser light at the beginning of the interaction. It is also assumed, but now only for this particular interaction, that the laser pulse is longer than the electron bunch, thus the entire electron bunch is energy modulated independent of jitter in the arrival time of the electron bunch in the wiggler magnet.

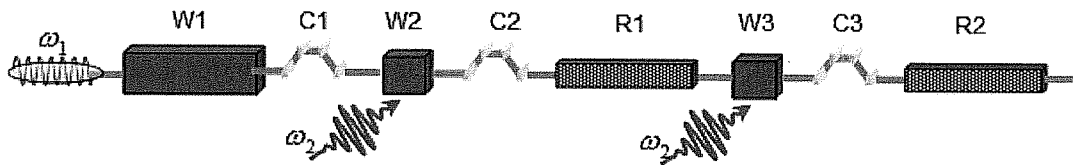


Figure 1. (Color online). A schematic of the generation of two attosecond x-ray pulses, where W1, W2 and W3 are wiggler magnets, C1, C2 and C3 are magnetic chicanes, R1 and R2 are x-ray undulator radiators, ω_1 is the carrier frequency of the long laser pulse and ω_2 is the carrier frequency of the short few-cycle laser pulse.

In the second step we send the energy-modulated electron bunch through a dispersive magnetic chicane C1 with a rather large time-of-flight parameter $R_{56}^{(1)}$ and achieve a characteristic electron distribution in the longitudinal phase space with a quasi equidistant spacing of narrow bands of electrons separated by similarly narrow bands of empty spaces (see illustration in Figure 2). This is a critical step that prepares the electrons for a following microbunching at a much shorter wavelength than λ_1 via transformation of a narrow spacing along the energy axis into the narrow spacing along the coordinate axis.

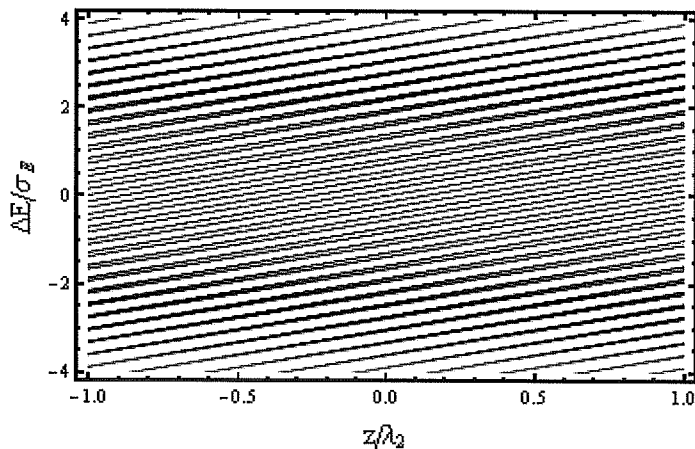


Figure 2. A fragment of the electron bunch longitudinal phase space after C1. Here and on other similar plots the horizontal axis is the distance along the bunch normalized to λ_2 and the vertical axis is energy deviation from the equilibrium energy normalized to the rms energy spread in the electron bunch.

As proposed in [15], this transformation is achieved by employing a second energy modulation of the electrons using the electron beam interaction with the laser field with a carrier frequency ω_2 in the second short wiggler magnet W2. The wiggler period

λ_{w2} and wiggler undulator parameter K_{w2} of this magnet has been chosen to match the FEL resonance at the wave length $\lambda_2 = 2\pi/q_2$, where $q_2 = \omega_2/c$ is the wave vector of the second laser field. This time the normalized amplitude of energy modulation $a_2 = \Delta E_2/\sigma_E$ is supposed to be large, of the order of 10-20. At this point we begin a selection process for the attosecond pulse. Therefore, we use a few-cycle laser pulse with carrier-envelope phase stabilization (see, for example, [2]) and a wiggler magnet with only one period, to apply the energy modulation in as short a section of the electron bunch as possible. The phase for the electric field in the center of the laser pulse is

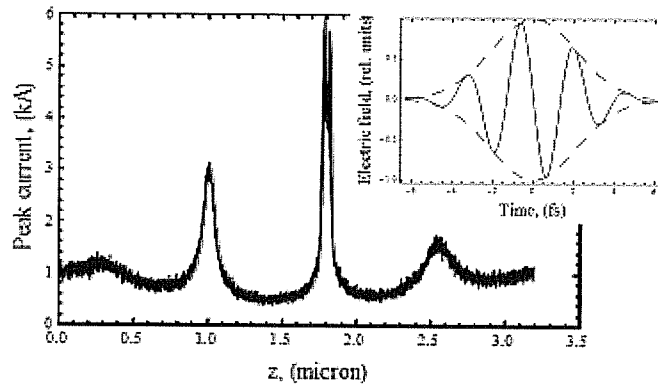


Figure 3. The enhancement in the electron peak current due to electron energy modulation in the interaction with a few-cycle laser pulse with carrier-envelope phase stabilization (see the insert).

adjusted to be zero when the center of the laser pulse passes the center of the wiggler magnet (see the insert in Figure 3). After the second wiggler, the electron bunch passes the second dispersive magnetic chicane C2 whose time-of-flight parameter $R_{56}^{(2)}$ is much smaller than $R_{56}^{(1)}$. As a result we obtain current enhancement shown in Figure 3 which is

large at the central peak and smaller at two side peaks (and absent everywhere else) [14]. At the same time the bands of electrons seen in Figure 2 rotate in the longitudinal phase space and appear on the coordinate axis as shown in Figure 4. This indicates an ultra fine microbunching structure of electrons inside the spikes of the peak current. For this to happen, one should carefully choose the combination of values of $R_{56}^{(1)}$, $R_{56}^{(2)}$ and a_2 . According to [15], the microbunching with a small period λ_{x1} corresponding to a harmonic number $h_1 = \lambda_2 / \lambda_{x1} = |n_1 + q_1/q_2|$ is strong when:

$$R_{56}^{(1)} q_1 \frac{a_2 \sigma_E}{E} \cong |n_1| + 0.809 |n_1|^{1/3} \quad (1)$$

$$R_{56}^{(2)} = -\frac{R_{56}^{(1)} q_1 - E / \sigma_E}{q_2 n_1 + q_1} \quad (2)$$

Here n_1 is a large positive or negative integer number. These equations can be used to define $R_{56}^{(1)}$, $R_{56}^{(2)}$ as a function of a_2 for a given h_1 , q_1 , q_2 and σ_E . We note that the conditions (1), (2) are carefully chosen to maximize the microbunching only inside the central spike of the peak current where we achieve the result that the narrow bands of electrons take a perfect upright position (see Figure 4a). At the same time, the same a_2 , $R_{56}^{(1)}$, $R_{56}^{(2)}$ are not optimal for the side peaks (see Figure 4b) and the microbunching there is much weaker than the microbunching inside the central current spike.

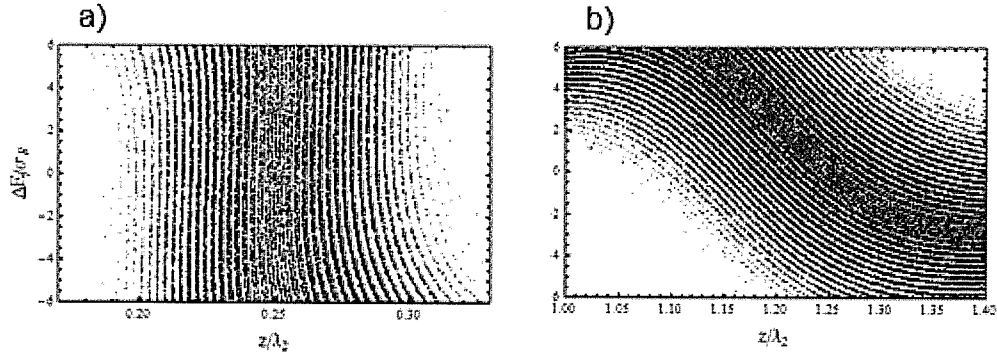


Figure 4. Two fragments of the electron bunch longitudinal phase space after C2 showing the microstructure inside a) the central peak and b) the side peak of Figure 3.

Following the generation of a narrow current spike, the electron bunch enters the undulator radiator R1 with period λ_{u1} and undulator parameter K_{x1} tuned for the FEL resonance at the wave length $\lambda_{x1} = \lambda_{u1} (1 + K_{x1}^2 / 2) / 2\gamma^2$. This undulator is relatively short because the central spike in the electron peak current is rather narrow, of the order of $\Delta z_1 = \lambda_2 a_1 / 2a_2$, and in the case of a large a_2 and a modest a_1 it can not provide a sustained support for the FEL process due to a slippage of the radiation field relative to electrons. All electrons radiate there, but electrons in the central peak (and to some extent the electrons in two side peaks) produce a short pulse of coherent radiation significantly enhanced by the high peak current and microbunching that dominates the radiation of the rest of the electron beam.

Having demonstrated how to obtain one attosecond x-ray pulse with the carrier wave length λ_{x1} , we now discuss generation of the second attosecond x-ray pulse with carrier wave length λ_{x2} . We employ a third energy modulation of the electrons using exactly the same laser pulse as for the second energy modulation what we plan to obtain

by splitting one parent few-cycle laser pulse with a carrier-envelop phase stabilization into two pulses and introducing an adjustable time delay. The wiggler magnet W3 is also the same design as W2. While passing through W3, electrons that overlap the second short pulse will acquire a large modulation amplitude a_3 of the order of 10-20 and will be located in a different section of the electron bunch than in the case of the energy modulation in W2. Following W3 is a third dispersive magnetic chicane C3. This time we adjust a_3 and time-of-flight parameter of this chicane $R_{56}^{(3)}$ to yield the microbunching at the wavelength λ_{x2} with the harmonic number $h_2 = \lambda_2 / \lambda_{x2} = |n_2 + q_1 / q_2|$ using similar constrains as in (1) and (2):

$$a_3 \cong \frac{|n_2| + 0.809|n_2|^{1/3}}{(R_{56}^{(1)} + R_{56}^{(2)})q_1\sigma_E / E} \quad (3)$$

$$R_{56}^{(3)} = -\frac{(R_{56}^{(1)} + R_{56}^{(2)})q_1 - E / \sigma_E}{q_2 n_2 + q_1} \quad (4)$$

Note that the cumulative time-of-flight parameter related to the energy bands is the sum $R_{56}^{(1)} + R_{56}^{(2)}$ from the two chicanes C1 and C2 which the beam has passed through up to this point. The final undulator radiator R2 has period λ_{u2} and undulator parameter K_{x2} tuned for the FEL resonance at the wave length λ_{x2} . Similar to R1, this is a relatively short undulator which is not intended to provide a sustained support for the FEL process because the central spike in the electron peak current is rather narrow, of the order of $\Delta z_2 = \lambda_2 a_1 / 2a_3$. The electrons in the central peak of the second section of the electron bunch have strong microbunching at the resonant wave length, and their radiation dominates the radiation from the rest of the electrons, including the electrons in the central peak of the first section of the electron bunch. The latter do not produce

significant coherent radiation in R2 because they have microbunching at λ_{x1} , which is the wrong wave length for this radiator.

3. Illustration

For a numerical illustration of the feasibility of the above described scheme we demonstrate generation of two attosecond x-ray pulses with one carrier frequency at the oxygen K-edge and the other carrier frequency at the nitrogen K-edge using the electron beam with the following parameters [16] listed in Table 1.

Table 1: The electron beam parameters

Electron beam energy	2.4 GeV
Electron beam peak current	1 kA
Slice emittance, rms	0.8 mm-mrad
Slice energy spread, rms	100 keV
Electron bunch length, FWHM	200 fs

In this section we often calculate the amplitude of energy modulation of electrons produced by the laser interaction with the electrons in the wiggler magnet using formula (9) from Ref. [17]:

$$\Delta E_L = 2\sqrt{A_L \alpha \hbar \omega \frac{K^2}{2 + K^2}} \left(J_0\left(\frac{1}{2} \frac{K^2}{2 + K^2}\right) - J_1\left(\frac{1}{2} \frac{K^2}{2 + K^2}\right) \right) f(\bar{q}, \nu, \bar{\sigma}_\tau) \quad (5)$$

$$f(\bar{q}, \nu, \bar{\sigma}_\tau) = \sqrt{\frac{2\bar{q}}{(2\pi)^{1/2} \bar{\sigma}_\tau}} \int_{-0.5}^{0.5} \frac{\cos(2\pi\nu\hat{s} - \tan^{-1}(\bar{q}\hat{s}))}{\sqrt{1 + (\bar{q}\hat{s})^2}} e^{-\hat{s}^2/4\bar{\sigma}_\tau^2} d\hat{s}$$

Where A_L is the laser pulse energy, $\alpha = 1/137$ is the fine structure constant, \hbar is the Planck's constant, J_0, J_1 are Bessel functions of the first kind, K is the wiggler undulator parameter, $\hat{s} = s/L_w$, where s is the coordinate along the wiggler and L_w is the length of the wiggler with N periods, $\nu = N2\delta\gamma/\gamma$ is detuning from the FEL resonance, $\hat{q} = L_w/z_R$ and z_R is the Rayleigh length, $\hat{\sigma}_\tau = \sigma_\tau/\tau_0$, where σ_τ is the rms laser pulse width and $\tau_0 = 2\pi N/\omega$, where ω is the laser frequency. These are general notations for all cases and in every specific case we use K, L_w, N, A_L, ω and z_R specific for that case. For example for energy modulation in W1 we use $N = 10$, $\lambda_{w1} = 16$ cm and $K_{w1} = 10.4$ and laser pulse with the carrier wave length of 200 nm, $\sigma_\tau = 800$ fs and $A_L = 5$ μ J focused in the wiggler center with $z_R = 43$ cm. In this case the ratio of the laser pulse waist w to the electron beam size σ_\perp is $w/\sigma_\perp = 4$, thus, energy modulation is practically insensitive to the electron transverse position. Using the above parameters we obtain $a_1 = 3$.

The downstream chicane C1 has $R_{56}^{(1)} = 17.63$ mm and consists of four bending magnets, each with length $L = 2.5$ m and bending angle $|\theta| = 63.8$ mrad, separated by 0.5 m long drift sections. Here we use rather long magnets in order to have small rms energy spread $\Delta\sigma_E$ induced by quantum fluctuation of synchrotron radiation [18]:

$$\frac{\Delta\sigma_E}{E} = \left(\frac{55}{48\sqrt{3}} \frac{r_e^2}{\alpha} \gamma^5 \theta^3 \right)^{1/2} \frac{1}{L}, \quad (6)$$

where r_e is the classical electron radius. Using (6) we calculate that each magnet contributes approximately 0.63 keV which is small compared to the distance between two adjacent bands of electrons in Figure 2, estimated to be $\delta E \approx E\lambda_1 / 2R_{56}^{(1)} = 13.6$ keV.

For a selective energy modulation of electrons within a few femtosecond long section of the electron bunch we employ a few-cycle laser pulse with carrier-envelope phase stabilization, a carrier wave length $\lambda_2 = 800$ nm and a pulse length of 3.5 fs (FWHM) for the intensity profile [19]. This pulse is divided into two pulses and the first one is used in W2 and the second one is used in W3. Both wigglers have $N = 1$, $\lambda_{w2} = 25$ cm and $K_{w2} = 16.7$. The first pulse with energy of 14 μ J is focused in the center of W2 with the Rayleigh length of 10.7 cm corresponding to $w = 4\sigma_{\perp}$ to produce energy modulation with the peak amplitude $a_2 = 16$. We note that the rms energy spread induced by synchrotron radiation in the wiggler magnet with large K is equal to [20]:

$$\frac{\Delta\sigma_E}{E} = \left(4.16 \frac{r_e^2}{\alpha} \gamma^2 N \left(\frac{eB}{mc} \right)^2 \right)^{1/2}, \quad (7)$$

In the case of W2 this amounts to 0.32 keV. By passing the electron bunch with this energy modulation through the chicane C2 with $R_{56}^{(2)} = 0.206$ mm consisting of four $L = 0.6$ m long bending magnets with bending angle $|\theta| = 10.1$ mrad separated by 0.6 m long drift sections we obtain the enhancement in the electron peak current (see Figure 3) and microbunching of electrons at the x-ray wave length $\lambda_{x1} = 2.27$ nm (see Figure 4a). Note that the plots in Figure 4 are obtained using a 1D particle tracking code which includes the effect of incoherent synchrotron radiation. The combination of parameters $R_{56}^{(1)}$, a_2 and $R_{56}^{(2)}$ has been chosen according to (1) and (2). Figure 5 shows the bunching

efficiency near to the main peak in Figure 3 calculated using 1D code. In the case of Figure 5 the step size $\Delta z = 3\lambda_2/44$ defines the slice of the electron bunch with the bunching factor:

$$b_k = \frac{1}{n_k} \sum_j^{n_k} e^{i\frac{2\pi}{\lambda_{x1}} z_j} \quad (8)$$

where n_k is the number of electrons located within the boundaries of the k-th slice.

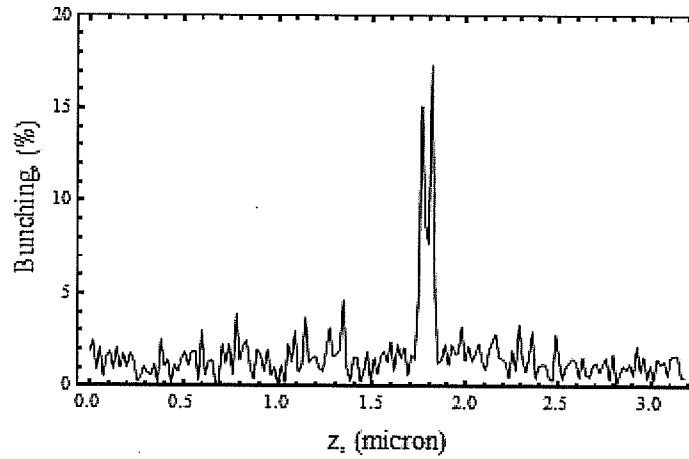


Figure 5. A fragment of the electron bunch showing bunching efficiency. Note, high bunching efficiency is seen only inside the main peak in the electron peak current.

Further downstream is the undulator radiator R1 with 40 periods, period length of 5 cm and undulator parameter $K_{x1} = 1.41$ tuned for the FEL resonance at the wave length λ_{x1} . Calculations carried out using GENESIS [21] with initial particle distribution prepared with 1D code show that when the electron bunch passes R1, the bunched electrons produce a dominant pulse of coherent x-ray radiation with 220 asec FWHM

shown in Figure 6. Because of the light emittance $\lambda_{x1}/4\pi$ is approximately equal to geometrical electron beam emittance, this radiation is transversely coherent.

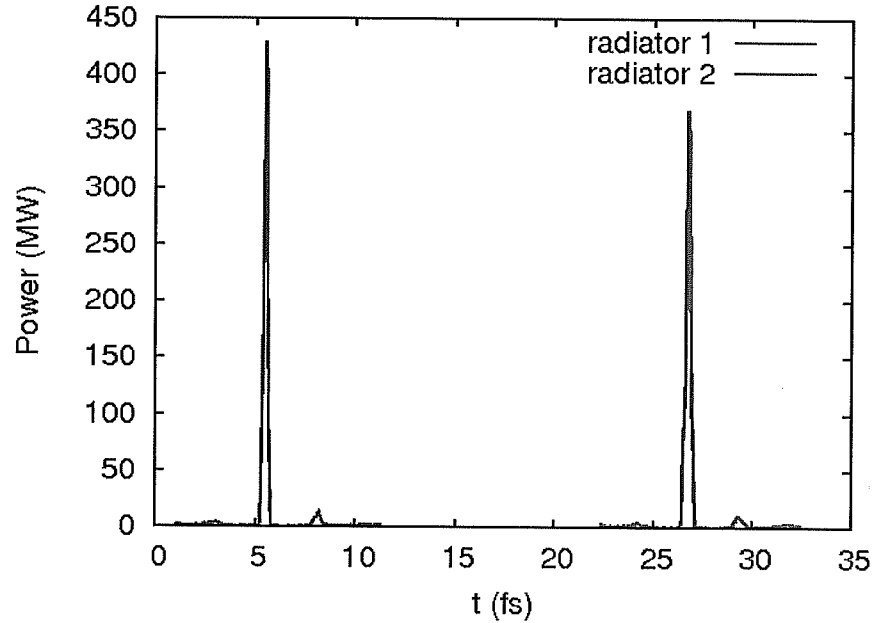


Figure 6. (Color online). Two x-ray pulses produced by the electron bunch radiating in the undulators R1 and R2. Note, coherent radiation of bunched electrons dominates spontaneous emission.

We use the second laser pulse in W3 in order to produce the second ultra-short pulse of coherent x-ray radiation with the carrier wave length $\lambda_{x2} = 3.03$ nm with a precisely controlled time delay with respect to the first x-ray pulse. According to Eq.(3) this laser pulse has to produce energy modulation of electrons with the peak amplitude $a_3 = 12.4$ corresponding to ~ 7 μ J laser pulse energy. After W3 the electron bunch passes the chicane C3 with $R_{36}^{(3)} = 0.267$ mm defined by Eq.(4). After that we obtain local enhancement in the electron peak current and microbunching of electrons at the x-ray

wave length $\lambda_{x2} = 3.03$ nm in a new section of the electron bunch. We note that C3 is identical to C2 except for a change in the bending angle $|\theta| = 11.6$ mrad.

The undulator radiator R2 is also identical to R1, but it is used with the undulator parameter $K_{x2} = 1.824$ for the FEL resonance at λ_{x2} . Here electrons in the second section of the electron bunch bunched at λ_{x2} produce the second pulse of coherent x-ray radiation with 260 asec FWHM shown in Figure 6. We note that the electrons from the first section do not produce large signal in R2 because they are bunched at the wrong wavelength for R2. In the above illustration the time delay between two attosecond pulses is arbitrary, but it can be easily adjusted through the time delay between two ultra-short laser pulses obtained from the same parent pulse. In the technique described above, the closest distance between two attosecond x-ray pulses can be as low as ~ 4 fs. This seems to be sufficient for experiments where the minimal interesting time delay between two x-ray pulses is defined by Auger process of the order of 5-10 fs. The maximum time delay is limited by the electron bunch length minus a jitter in the electron bunch arrival time with respect to the timing of the ultra-short laser pulse and can easily be of the order of 150 fs. Finally, Figure 7 shows the spectrum of the signal comprised of two ultra-short x-ray pulses shown in Figure 6. The x-ray pulse at 544 eV has 8.5 eV FWHM and 102 nJ pulse energy in the spectral peak and the x-ray pulse at 405 eV has 6.6 eV FWHM and 114 nJ pulse energy in the spectral peak. Near to this peak there is also a small side peak with 3 nJ total energy.

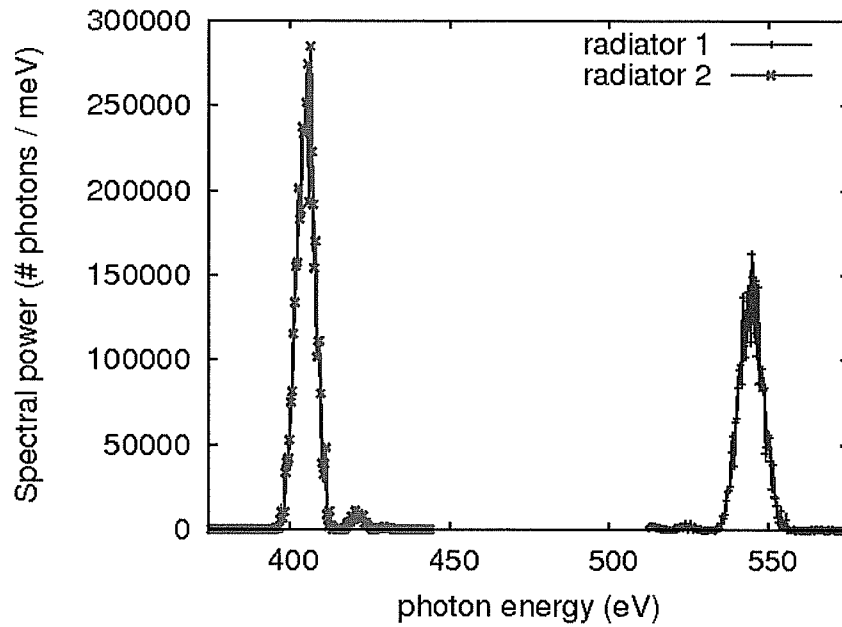


Figure 7. (Color online). The spectrum of two x-ray pulses produced by the electron bunch radiating in the undulators R1 and R2. Pulse intensity on the vertical axis is given in units of number of photons per meV.

4. Summary

Two powerful attosecond x-ray pulses can be produced in an FEL using two different sections of the electron bunch interacting with ultra-short laser pulses. Here, we demonstrate that by employing the technique of echo-enabled harmonic generation one can actually tune carrier frequencies of these pulses to different values independently from each other. The time delay between these pulses is not affected by jitter in the electron bunch arrival time and can be strictly controlled with high precision as both pulses are synchronized to a single parent laser pulse. All the above listed features are

essential for the study of the processes of making or breaking chemical bonds in molecules using x-ray stimulated Raman spectroscopy.

This work was supported by U.S. DoE under contract No: DE-AC02-05H11231. One of us (AZ) is very grateful to I. Schweigert, S. Mukamel and W. McCurdy for useful discussions.

References

- [1] A.H. Zewail, *J. Phys. Chem. A*, **104**, 5660(2000).
- [2] F. Krausz and M. Ivanov, *Reviews of Modern Phys.*, **81**, 163(2009).
- [3] E.L. Saldin, E.A. Schneidmiller, M.V. Yurkov, *Opt. Commun.* **212**, 377 (2002).
- [4] A.A. Zholents and W.M. Fawley, *Phys. Rev. Lett*, **92**, 224801 (2004).
- [5] P. Emma, K. Bane, M. Cornacchia, Z. Huang, H. Schlarb, G. Stupakov and D. Walz, *Phys. Rev. Lett*, **92**, 074801 (2004).
- [6] E.L. Saldin, E.A. Schneidmiller, and M.V. Yurkov, *Opt. Commun.* **239**, 161 (2004).
- [7] A.A. Zholents and G. Penn, *Phys. Rev. ST Accel. Beams*, **8**, 050704 (2005).
- [8] E.L. Saldin, E.A. Schneidmiller, and M.V. Yurkov, *Phys. Rev. ST Accel. Beams*, **9**, 050702(2006).
- [9] A.A. Zholents and M.S. Zolotarev, *New J. Phys*, **10**, 025005 (2008).
- [10] S. Reiche, P. Musumeci, C. Pellegrini and J.B. Rosenzweig, *Nucl. Inst. Methods Phys. Res., Sect. A* **593**, 45 (2008).
- [11] Y. Ding, Z. Huang, D. Ratner, P. Bucksbaum and H. Merdji, *Phys. Rev. ST Accel. Beams*, **12**, 060703(2009).

- [12] D. Xiang, Z. Huang and G. Stupakov, Phys. Rev. ST Accel. Beams, **12**, 060701(2009).
- [13] I. V. Schweigert and S. Mukamel, Phys. Rev. A **76**, 012504(2007).
- [14] A. Zholents, Phys. Rev. ST AB, **8**, 040701, 2005.
- [15] G. Stupakov, Phys. Rev. Lett., **102**, 074801(2009).
- [16] A.A. Zholents, E. Kur, G. Penn, Ji Qiang, M. Venturini, R. P. Wells, to be published in Proc. of Linac conference, Victoria, Canada, 2008.
- [17] A. Zholents and K. Holldack, Proc. Free Electron Laser Conf. 2006, Berlin, (2006).
- [18] A.W. Chao and M. Tigner, Handbook of Accelerator Physics and Engineering, World Scientific, Singapore, 2006.
- [19] A. L. Cavalieri, E. Goulielmakis, B. Horvath, W. Helml, M. Schultze, M. Fieß, V. Pervak, L. Veisz, V. S. Yakovlev, M. Uiberacker, A. Apolonski, F. Krausz, R. Kienberger, New J. of Phys, **9**, 242(2007).
- [20] E. Saldin, E. Schneidmiller and M. Yurkov, Nucl. Instr. Meth. Phys. Res. A, **381**, 545(1996).
- [21] S. Reiche, Nucl. Instrum. Methods Phys. Res. A **429**, 243 (1999).